Available online at www.sciencedirect.com
ScienceDirect
Trans. Nonferrous Met. Soc. China 31(2021) 2787−2796
Transactions of Nonferrous Metals Society of China
www.tnmsc.cn

Fatigue analysis of closed-cell aluminium foam using different material models

M. ULBIN, S. GLODEŽ

Faculty of Mechanical Engineering, University of Maribor, Smetanova 17, 2000 Maribor, Slovenia

Received 13 October 2020; accepted 15 April 2021

Abstract: The fatigue analyses of AlSi7 closed-cell aluminium foam were performed using a real porous model and three different homogenised material models: crushable foam model, isotropic hardening model and kinematic hardening model. The numerical analysis using all three homogenised material models is based on the available experimental results previously determined from fatigue tests under oscillating tensile loading with the stress ratio R=0.1. The obtained computational results have shown that both isotropic and kinematic hardening models are suitable to analyse the fatigue behaviour of closed-cell aluminium foam. Besides, the kinematic hardening material model has demonstrated significantly shorter simulation time if compared to the isotropic hardening material model. On the other hand, the crushable foam model is recognized as an inappropriate approach for the fatigue analyses under tension loading conditions.

Key words: closed-cell aluminium foams; fatigue; numerical analysis; material model

1 Introduction

Metal foams are advanced engineering materials characterised by low density and novel physical, mechanical, thermal and acoustic properties [1−4]. For that reason, metal foams offer great potential in many engineering applications, such as lightweight structures, energy absorbers, automotive and aircraft industry [5−7]. As presented by SHEN et al [8], KASHEF et al [9] and GAIN et al [10], metal foams may also be used in different medical applications (e.g. replacement of damaged bones). Applications, where metal foams are used, may at first be highly specialized, but, as production volume increases and costs decrease, widespread adoption of metal foams is possible [11,12].

In recent years, a great effort has been put into aluminium foams due to their low weight and low melting points as well as the relatively good ductility and formability, excellent corrosion resistance and recycling potential [13−15]. Al-alloy foams are usually used in the form of closed-cell structures produced by powder metallurgy (PM) technology using direct or indirect foaming methods [16,17]. Up to date, an extensive investigation has been performed to characterize the mechanical properties of closed-cell aluminium foams under quasi-static or impact loading conditions. DUARTE et al [18], GERAMIPOUR and OVEISI [19], AVALLE et al [20] and SAADATFAR et al [21] studied the mechanical behaviour of closed-cell aluminium foam under uniaxial quasi-static compressive loading. Their results showed a significant increase in the collapse stress of the porous structure when radial constraints are applied. Furthermore, the strain hardening occurred predominantly in regions with large cells and high anisotropy of an examined porous structure. RUAN et al [22] and ZHOU et al [23] compared the mechanical behaviour of

Corresponding author: M. ULBIN, Tel: +386-2-2207705, Fax: +386-2-2207994, E-mail: miran.ulbin@um.si
DOI: 10.1016/S1003-6326(21)65693-5

closed-cell aluminium foams under quasi-static uniaxial tensile and uniaxial compression. They concluded that aluminium foams exhibit less ductility in tension than compression. As mentioned above, closed-cell aluminium foams are often used as a high-energy absorber where dynamic (impact) loading appears [24]. SALEHI et al [25], SHEN et al [26] and JANG et al [27] investigated the compressive behaviour of closed-cell aluminium foams by impact loading. Based on their experimental results, it can be established that closed-cell aluminium foam is a strain rate sensitive material.

However, there are minimal investigations regarding the fatigue behaviour of closed-cell aluminium foams. SCHULTZ et al [28] investigated the fatigue behaviour of different aluminium foams experimentally under completely reversed loading (stress ratio R=−1). They concluded that the scatter of the foam densities led to the scatter of the fatigue life of the analysed porous structure. ZHAO et al [29] proposed the experimental investigation of the fatigue of closed-cell aluminium foam under pulsating tension. The obtained S–N curve shows a large scatter, which is a consequence of the irregularity of the inner foam structure. As presented by the same author [30], fatigue life decreases as the number and the size of large cells increase. The experimental investigation of the fatigue behaviour of closed-cell aluminium foam under pulsating compression was performed by KOLLURI et al [31]. Their results have shown that the fatigue behaviour of Al-foams is relatively less sensitive to morphological defects such as missing walls than the quasi-static mechanical properties such as plastic strength. LINUL et al [32] investigated the effect of the morphology (the number and the size of cells) on the fatigue response of ductile closed-cell aluminium foam in a low cycle fatigue regime. Their study has shown that fatigue life decreases as the number and the size of large cells increase, which is in accordance with the survey proposed by ZHAO et al [29,30] and investigation proposed by LIU and DU [33]. INGRAHAM et al [34] studied the low cycle fatigue behaviour of Al-foam under tension−compression loading conditions. They concluded that the low-cycle fatigue behaviour of closed-cell Al-foam might be described with the Coffin–Manson relationship, which provides a preliminary design tool for this type of engineering material. OLURIN et al [35] and FAN et al [36] proposed the experimental research on the fatigue crack propagation in aluminium alloy foams using CT-specimens to determine the Paris curve. The experimental results have shown that increasing the mean applied stress increases the Paris-law exponent and, for a given stress intensity range ΔK, increases the crack growth rate da/dN. An experimental investigation by MOTZ et al [37] has shown that the closed-cell aluminium foam demonstrates relatively high Paris-exponent m if compared to common ductile solid metals. The similar work has also been proposed by AMSTERDAM et al [38]. Besides the experimental investigations, some computational studies have been performed to simulate the failure mechanisms of closed-cell aluminium foam. However, most of these studies are related to the numerical simulations under quasi-static (VENGATACHALAM et al [39] and NAMMI et al [40]) or crush loading (CZEKANSKI et al [41] and KADER et al [42]).

In the present study, the computational fatigue analysis of closed-cell aluminium foam using different homogenised material models is presented. The used material models are based on the previous experimental testing on tensile specimens made of closed-cell aluminium foams [43] where an inverse procedure was implemented to determine the required material parameters.

2 Experimental

The specimens made of AlSi7 closed-cell aluminium foam were prepared using PM process, as described in Ref. [43]. The geometry of the cylindrical specimen is shown in Fig. 1(a). Figure 1(b) shows the porous structure of the specimen with the average porosity p≈0.76, which has been determined previously using micro CT-scans.

The material models are based on the available experimental results from static and fatigue tests made on the cylindrical porous specimens made of the examined closed-cell aluminium foam. Figure 2(a) shows the static stress−strain curve, where the stress is related to the nominal cross-section of the specimen (A_{nom}≈491 mm^2; see Fig. 1). Figure 2(b) shows the cyclic stress−strain

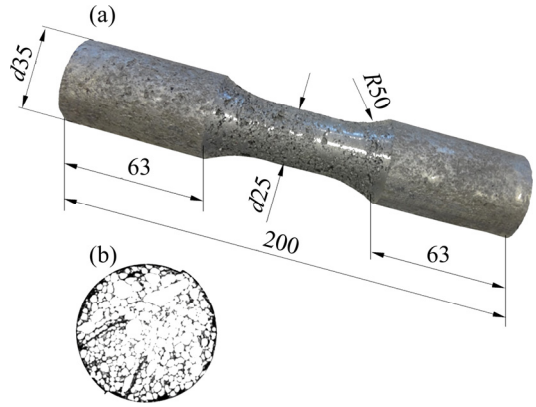

Fig. 1 Test specimen: (a) Geometry of specimen (unit: mm); (b) Porous structure of specimen

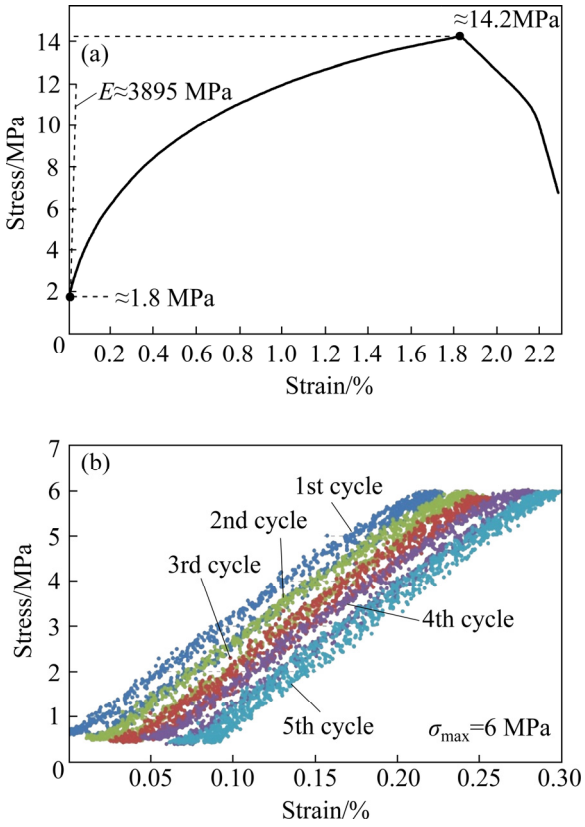

Fig. 2 Static (a) and cyclic (b) stress−strain curves of closed-cell aluminium foam

curves for the first five stress cycles under maximum nominal stress of 6 MPa and stress ratio R=0.1. The similar fatigue tests have also been done for the stress levels of 4 and 8 MPa. Three specimens were tested for each stress level (4, 6 and 8 MPa). During testing, the machine was force controlled, recording tensile force, strain and the number of stress cycles until fracture (the detailed experimental procedure is described in Ref. [43]). The experimental results of the fatigue tests are presented in Table 1. The porosity of specimens was in the range of 0.75−0.77, with an average porosity of 0.76. A relatively large scatter of experimentally determined fatigue life is evident, which is undoubtedly due to the inhomogeneous structure, surface irregularities, different porosities and different pore sizes of analysed porous specimens. Specimens with lower porosity have recorded longer fatigue life than specimens with higher porosity. The obtained experimental results are comparable to the experimental results published by ZHAO et al [30], who investigated the fatigue damage of similar closed-cell aluminium foam as presented in this study. However, they used dog-bone specimens instead of cylindrical specimens as already described above.

Table 1 Experimental results for fatigue tests

Force, F_{max}/kN	Maximum nominal stress, σ_{max}/MPa	Fatigue life, N		
		Test 1	Test 2	Test 3
4.175	8	80	2	1
2.995	6	12	424	77
2.115	4	16500	47000	26600

Figure 3 shows the experimentally determined strain−life curve (Coffin−Manson curve) of the examined closed-cell aluminium foam, from which the fatigue life N can be obtained. The strain−life curve in Fig. 3 is constructed with consideration of experimentally determined number of stress cycles up to specimen failure N (see Table 1) and the total strain range $\Delta\varepsilon$, which is in this study obtained using the appropriate material model.

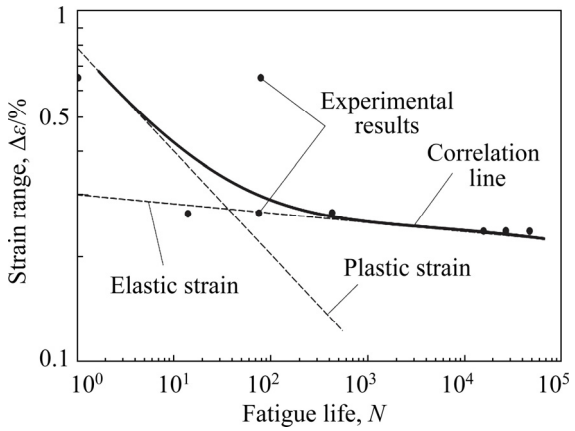

Fig. 3 Strain−life curve of examined closed-cell aluminum foam

3 Fatigue life estimation

Fatigue life estimation of porous materials as metal foams is in general challenging to process because a comprehensive computational analysis using numerical models with a vast number of finite elements is required for that purpose. Instead of modelling the exact internal structure of an examined porous material, an appropriate homogenised material model can be performed in the subsequent numerical analysis.

3.1 Porous model

In the porous model, reverse engineering techniques were used to create a numerical model of the porous specimen shown in Fig. 1. The numerical model was created from the solid material part where spherical pores were cut out at the exact positions of pores previously obtained from computer tomography scans. In the numerical model (Fig. 4), a specimen was fixed on the bottom side (z=0), and cyclic tensile displacement was applied at the top surface of the specimen. Nonlinear elastic-plastic numerical analysis has then been performed using material parameters given in Table 2. The obtained strains then serve as a basis for the subsequent fatigue analysis in the framework of FE-Safe software [45], where the fatigue lives were determined using maximum shear strain criterion with consideration of the Morrow mean stress correction.

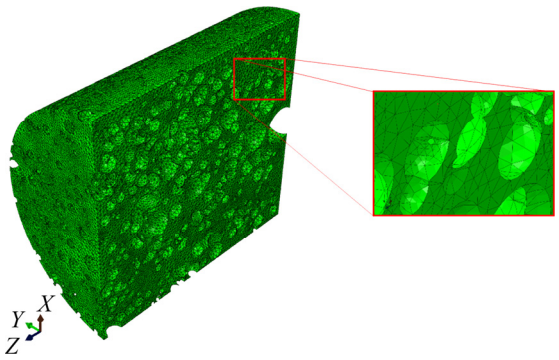

Fig. 4 3D-model of specimen with porosity p=0.52

The porosity of the model presented in Fig. 4 is 0.52, while the actual sample of material has a porosity of 0.76. For that reason, we also made computational analyses for porosities of 0.13 and 0.35. Models with reduced porosities do not reflect real-world material. Models included large pores, but it was not possible to model the majority of tiny pores. Figure 5 represents a function between the porosity p and appropriate reaction force F. The real reaction force extrapolates to F=2.672 kN for the actual porosity p=0.76, which corresponds to the fatigue life of approximately 1500 loading cycles.

3.2 Crushable foam model

The crushable foam model was developed from mechanical experiments with open- and closed-cell aluminium foams. The yield surface was found to be of elliptic shape in the effective stress−hydrostatic stress space and to be symmetric with respect to the axes, and it can be described with two independent parameters. The homogenized crushable foam model implemented in the finite element software Abaqus is based on the model presented by DESPANDE and FLECK [46]. The yield surface in the Abaqus model is not assumed to be symmetric to the effective stress axis, so it can be considered as a generalization of the original model. The yield surface is defined by two parameters describing the ratio between hydrostatic tensile yield strength and hydrostatic compressive yield strength and the ratio between the semi-major axis and the semi-minor axis of the ellipse. For volumetric or isotropic hardening description, uniaxial stress−strain data are required.

The crushable foam model is primarily suitable for the compressive loading, as hardening is based entirely on the material response to uniaxial compression [10]. In the case of the pure tension (oscillating tensile loading with the stress ratio R=0.1), it was impossible to simulate the cycling loading due to convergence problems in the first loading cycle, when the load exceeded the

Table 2 Material properties of aluminium alloy AlSi7 [44]

Elastic modulus, E/MPa	Poisson ratio	Yield stress/MPa	σ−ε curve		Strain−life curve			
			H'	n'	σ_f'/MPa	b	ε_f'	C
70000	0.33	411	655	0.065	1103	−0.124	0.22	−0.59

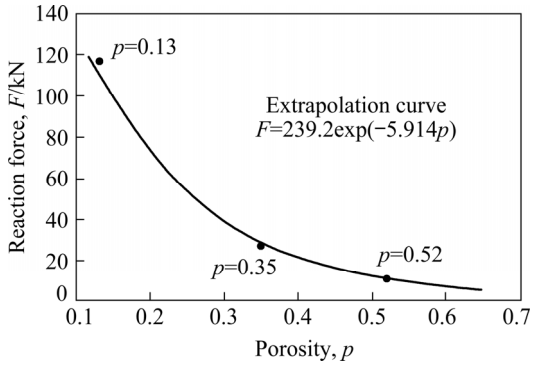

Fig. 5 Extrapolated reaction forces regarding different porosities

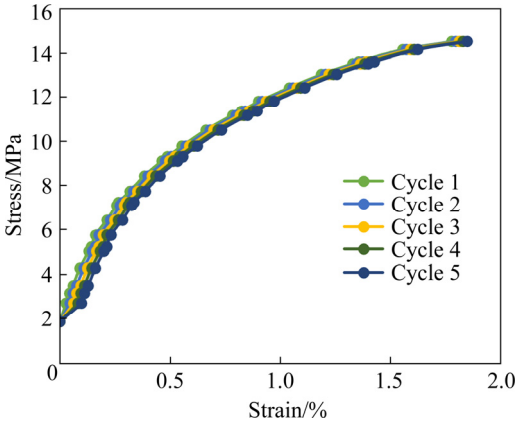

Fig. 6 Isotropic material data

elastic threshold of the material. Therefore, only results for minimal tensile loads were obtained, resulting in the elastic behaviour of the model. For that reason, the crushable foam model is inappropriate for analysing the fatigue problems under tensile loading.

3.3 Isotropic hardening material model

The isotropic hardening material model is based on the experimental results of the analysed structure, which are for the examined specimen presented in Fig. 2. In this model, the plasticity is defined as a functional relationship between the yield stress σ^0 and the equivalent plastic strain $\bar{\varepsilon}^{pl}$ using the following equation:

$$\sigma^0=f(\bar{\varepsilon}^{pl},\theta) \quad (1)$$

where θ is the temperature which can in this model be considered as a variable. The function f in Eq. (1) is defined using a previously determined static and cycling stress−strain curve shown in Fig. 2. The yield stress, σ^0, is given as a tabular function of plastic strain and temperature, where each temperature variable defined a different loading cycle. The strains for each cycle in Fig. 6 were, therefore, shifted to fit the experimental data, and to simulate the ratcheting effect, as shown in Fig. 2(b).

In this approach, the cyclic displacement was applied to one side of the specimen (see Fig. 7). For control of the exact external loading, the reaction forces were measured in the reference point on the other side of the specimen.

Figure 8 shows the equivalent stresses and strains after the last loading cycle for the applied maximum tensile load of 2.995 kN. As the plastic deformation occurs, it can be expected that the

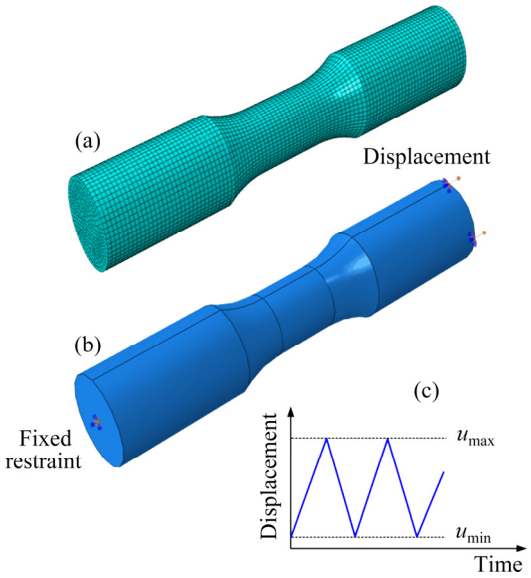

Fig. 7 Numerical model of specimen: (a) Finite element mesh; (b) Boundary conditions; (c) Pattern of cyclic displacement

specimen will fail after a reasonable number of loading cycles. By considering the assumption that the numerically determined equivalent strain corresponds to the total strain range $\Delta\varepsilon$, the associated fatigue life can then be obtained from the strain–life curve in Fig. 3. Similar numerical simulations have also been done for other external loadings, and results are summarised in Fig. 9.

The significant weakness of this approach is a considerable amount of simulation time required for the numerical simulation (several CPU hours were needed when analysing the specimen presented in Fig. 7). Although the obtained numerical results are in a reasonable agreement with the experimental results, the enormous simulation time can be expected when analysing the real engineering components made of the examined porous structure.

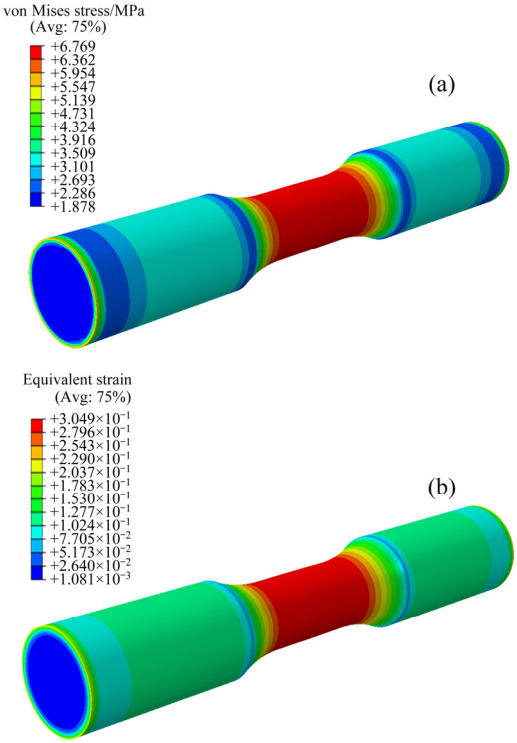

Fig. 8 Equivalent stress (a) and equivalent strain (b) for applied tensile load F_{max}=2.995 kN by isotropic hardening material model

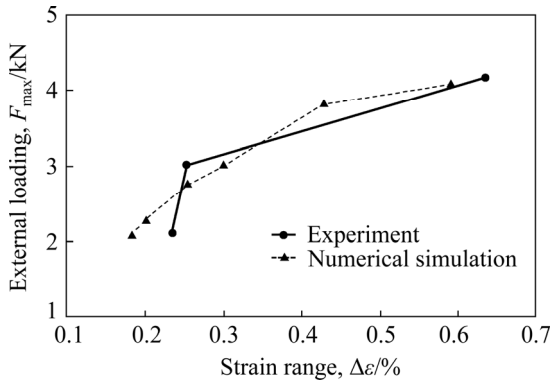

Fig. 9 Comparison between experimentally and numerically determined strain range $\Delta\varepsilon$ by isotropic hardening material model

3.4 Kinematic hardening material model

Alternatively, as to the isotropic hardening material model, a kinematic hardening model could be used, as presented by OKOROKOV et al [47]. As stress−strain curve of the examined closed-cell aluminium foam is available, it was possible to obtain the data for combined kinematic hardening approach (see Abaqus MIT [48]). From stress−strain pairs, the backstresses α_i can be calculated from Eq. (2):

$$\alpha_i=\sigma_i+\sigma_i^0 \tag{2}$$

where σ_i is the arbitrary stress and σ_i^0 is the yield stress.

The kinematic hardening is defined with the parameter α_k which should approach the backstress α_i (the maximum difference between α_k and α_i should be less than 15%):

$$\alpha_k=\frac{C_k}{\gamma_k}[1-\exp(-\gamma_k\cdot\varepsilon^{pl})] \tag{3}$$

Parameters C_k and γ_k can be evaluated as follows:

$$C_k=\frac{\sigma_k-\sigma_i^0}{\varepsilon_k^{pl}} \tag{4}$$

$$\gamma_k=\frac{-\ln\left(1-\dfrac{\sigma_k-\sigma_i^0}{C_k}\right)}{\varepsilon_k^{pl}} \tag{5}$$

Kinematic hardening, as described above, does not solve the ratcheting effect from the experimental testing (see Fig. 2). Therefore, the experimental data from the static tension test should be shifted by ratcheting strains, as obtained from experimental fatigue tests. Based on this assumption, the appropriate homogenized material model of the examined closed-cell aluminium foam can be constructed (see Fig. 10).

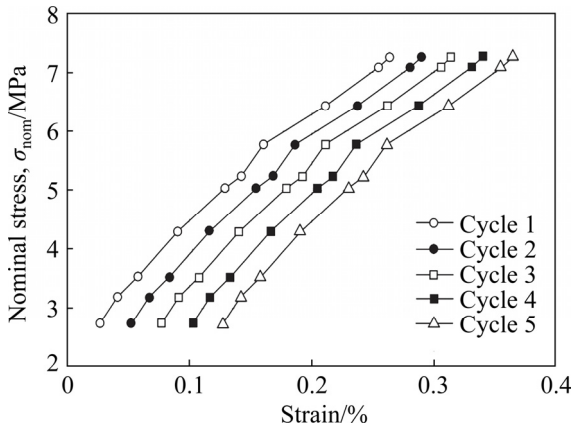

Fig. 10 Homogenized material model of examined closed-cell aluminium foam for F_{max}≈2.995 kN

Figures 11 shows the equivalent stresses and strains after the last loading cycle for the applied maximum tensile load of 2.995 kN. Similar numerical simulations have also been done for other external loadings, and results are summarised in Fig. 12. In the subsequent computational analyses, the numerically determined strain ranges $\Delta\varepsilon$ were

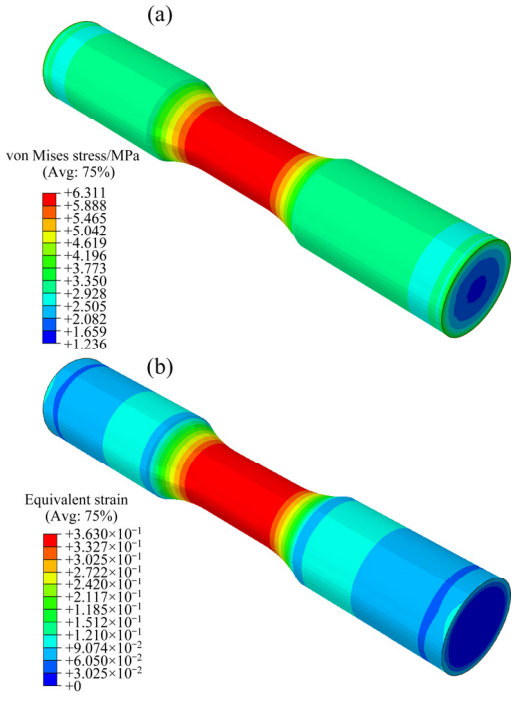

Fig. 11 Equivalent stress (a) and equivalent strain (b) for applied tensile load F_{max}=2.995 kN by kinematic hardening material model

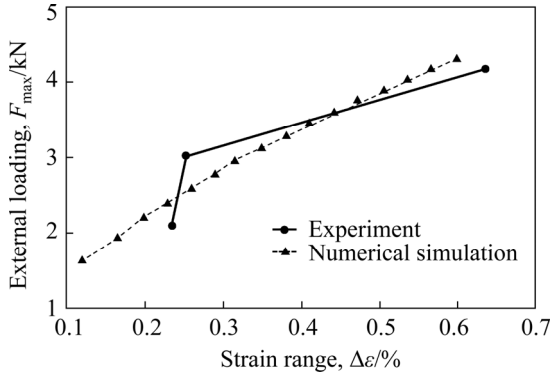

Fig. 12 Comparison between experimentally and numerically determined strain range $\Delta\varepsilon$ by kinematic hardening material model

used to obtain the fatigue life of the examined specimens made of closed-cell aluminium from the strain–life curve in Fig. 3.

Numerical simulations using the kinematic hardening material model have shown significantly shorter simulation time (only 10 CPU minutes per simulation) if compared to the isotropic hardening material model.

3.5 Results and discussion

Table 3 shows the comparison between experimentally and numerically determined fatigue life of the examined porous specimen made of closed-cell aluminium foam. The results are given for three different external loadings (F_{max}=2.115, 2.995 and 4.175 kN) which were considered by experimental testing. However, in the case of a porous model (see Section 3.1), the fatigue life is given only for the external loading F_{max}=2.67 kN.

It is evident from Table 3 that only the computational results according to the isotropic and kinematic hardening model can be qualitatively compared to the experimental results. Namely, the computational analysis using the porous model has been performed only for the external loading of 2.67 kN (the obtained fatigue life N=1500 loading cycles fall into the area of experimental results). Besides that, the computational analysis using Crushable foam model did not converge because of complete tensile loading of the examined specimen. On the other hand, the computational results for both isotropic and kinematic hardening models are in a reasonable agreement with the experimental results, especially in the area of low cycle fatigue (high loading, and large plastic deformation).

4 Conclusions

(1) Crushable foam model is not suitable for the tension loading. Namely, it was impossible to simulate the cycling loading in the case of the pure tension (the stress ratio R=0.1 considered in this simulation) due to the convergence in the first loading cycle.

Table 3 Experimentally and numerically determined fatigue life of examined porous specimen

External loading, F_{max}/kN	Number of cycles to failure, N				
	Experimental testing	Porous model	Crushable foam model	Isotropic hardening model	Kinematic hardening model
4.175	1−80	1500 (F_{max}=2.67 kN)	Convergence problems	≈3	≈18
2.995	12−424			≈80	≈900
2.115	16500−47000			$>10^5$	$>10^5$

(2) The obtained computational results have shown that both isotropic and kinematic hardening models are suitable to analyse the fatigue behaviour of closed-cell aluminium foam. However, the kinematic hardening material model has demonstrated significantly shorter simulation time (only 10 CPU minutes per simulation) if compared to the isotropic hardening material model (several CPU hours needed for each numerical simulation). For that reason, it is proposed to use the kinematic hardening material model when analysing the fatigue behaviour of real engineering components made of closed-cell aluminium foam.

(3) Although the required material parameters were determined using a relatively small number of test specimens, the comparison between experimentally and numerically determined strain ranges and fatigue lives shows a reasonable agreement. Based on the stochastic nature of the examined material, a large number of experiments and simulations would be necessary to obtain the required material parameters more accurately.

Acknowledgments

The authors would like to thank the Ministry of Education, Science, and Sport of the Republic of Slovenia for financial support (Research Core Funding No. P2-0063).

Data availability

The raw/processed data required to reproduce these findings cannot be shared at this time due to technical or time limitations.

References

[1] ASHBY M F, EVANS A, FLECK N A, GIBSON L J, HUTCHINSON J W, WADLEY H N G. Metal foams: A design guide [M]. Oxford: Butterworth-Heinemann, 2000.

[2] GIBSON L J, ASHBY M F. Cellular solids: Structure and properties [M]. Cambridge: Cambridge University Press, 1997.

[3] WANG N Z, CHEN X, LI A, LI Y X, ZHANG H W, LIU Y. Three-point bending performance of a new aluminum foam composite structure [J]. Transactions of Nonferrous Metals Society of China, 2016, 26: 359−368.

[4] LIU P S, MA X M. Property relations based on the octahedral structure model with body-centered cubic mode for porous metal foams [J]. Materials and Design, 2020, 188: 108413.

[5] DEGISCHER H P, KRISZT B. Handbook of cellular metals: Production, processing, applications [M]. Weinheim: Wiley, 2002.

[6] LI Z B, LI X Y, ZHENG Y X. Biaxial mechanical behaviour of closed-cell aluminum foam under combined shear-compression loading [J]. Transactions of Nonferrous Metals Society of China, 2020, 30: 41−50.

[7] LIU P, CHEN G F. Porous materials: Processing and Applications [M]. Elsevier, 2014.

[8] SHEN H, OPPENHEIMER S M, DUNALD D C, BRINSON L C. Numerical modelling of pore size and distribution in foamed titanium [J]. Mechanics of Materials, 2006, 38: 933–944.

[9] KASHEF S, ASGARI A, HILDITCH T B, YAN W, GOEL V K, HODGSON P D. Fatigue crack growth behaviour of titanium foams for medical applications [J]. Materials Science and Engineering A, 2011, 528: 1602−1607.

[10] GAIN A K, ZHANG L, QUADIR M Z. Composites matching the properties of human cortial bones: The design of porous titanium−zirconia (Ti−ZrO_2) nanocomposites using polymethyl methacrylate powders [J]. Materials Science and Engineering A, 2016, 662: 258−267.

[11] FIEDLER T, TAHERISHARGH M, KRSTULOVIĆ-OPARA L, VESENJAK M. Dynamic compressive loading of expanded perlite/aluminum syntactic foam [J]. Materials Science and Engineering A, 2015, 626: 296−304.

[12] LEHMHUS D, VESENJAK M, SCHAMPHELEIRE S D, FIEDLER T. From stochastic foam to designed structure: Balancing cost and performance of cellular metals [J]. Materials, 2017, 10: 922.

[13] HUANG R X, MA S Q, ZHANG M D, XU J J, WANG Z Y. Dynamic deformation and failure process of quasi-closed-cell aluminium foam manufactured by direct foaming technique [J]. Materials Science and Engineering A, 2019, 756: 302−311.

[14] PETIT C, MAIRE E, MEILLE S, ADRIEN J. Two-scale study of the fracture of an aluminium foam by X-ray tomography and finite element modelling [J]. Materials & Design, 2017, 120: 117−127.

[15] DUARTE I, VESENJAK M, KRSTULOVIĆ-OPARA L. Dynamic and quasi-static bending behaviour of thin-walled aluminium tubes filled with aluminium foam [J]. Composite Structures, 2014, 109: 48−56.

[16] DUARTE I, VESENSAK M, KRSTULOVIC-OPARA L, ANŽEL I, FERREIRA J M F. Manufacturing and bending behaviour of in situ foam-filled aluminium alloy tubes [J]. Materials & Design, 2015, 66: 532–544.

[17] KÖRNER C, ARNOLD-SINGER R F. Metal foam stabilization by oxide network particles [J]. Materials Science and Engineering A, 2005, 396: 28−40.

[18] DUARTE I, VESENJAK M, KRSTULOVIĆ-OPARA L. Compressive behaviour of unconstrained and constrained integral-skin closed-cell aluminium foam [J]. Composite Structures, 2016, 154: 231−238.

[19] GERAMIPOUR T, OVEISI H. Effects of foaming parameters on microstructure and compressive properties of aluminium foams produced by powder metallurgy method [J]. Transactions of Nonferrous Metals Society of China, 2017, 27: 1569−1579.

[20] AVALLE M, LEHMHUS D, PERONI L, PLETEIT H, SCHMIECHEN P, BELINGARDI G, BUSSE M. AlSi7 metallic foams – Aspects of material modelling for crash

analysis [J]. International Journal of Crashworthiness, 2009, 14: 269−285.

[21] SAADAFTAR M, MUKLHERJEE M, MADADI M, SCHRÖDER-TURK G E, GARCIA-MORENO F, SCHALLER F M, HUTZLER S, SHEPPARD A P, BANHART J, RAMAMURTY U. Structure and deformation correlation of closed-cell aluminium foam subject to uniaxial compression [J]. Acta Materialia, 2012, 60: 3604−3615.

[22] RUAN D, LU G, ONG L S, WANG B. Triaxial compression of aluminium foams [J]. Composites Science and Technology, 2007, 67: 1218−1234.

[23] ZHOU Z W, WANG Z H, ZHAO L M, SHU X F. Uniaxial and biaxial failure behaviours of aluminium alloy foams [J]. Composites Part B: Engineering, 2014, 61: 340−349.

[24] WANG Z H, JING L, ZHAO L M. Elasto-plastic constitutive model of aluminium alloy foam subjected to impact loading [J]. Transactions of Nonferrous Metals Society of China, 2011, 21: 449−454.

[25] SALEHI M, MIRBAGHERI S M H, JAFARI RAMIANI A. Efficient energy absorption of functionally-graded metallic foam-filled tubes under impact loading [J]. Transactions of Nonferrous Metals Society of China, 2021, 31: 92−110.

[26] SHEN J H, LU G X, RUAN D. Compressive behaviour of closed-cell aluminium foams at high strain rates [J]. Composites Part B: Engineering, 2010, 41: 678−685.

[27] JANG W Y, HSIEH W Y, MIAO C C, YEN Y C. Microstructure and mechanical properties of ALPORAS closed-cell aluminium foam [J]. Materials Characterization, 2015, 107: 228−238.

[28] SCHULTZ O, DES LIGNERIS A, HAIDER O, STARKE P. Fatigue behaviour, strength, and failure of aluminium foam [J]. Advanced Engineering Materials, 2000, 2: 215−218.

[29] ZHAO M D, FAN X, FANG Q Z, WANG T J. Experimental investigation of the fatigue of closed-cell aluminium alloy foam [J]. Materials Letters, 2015,160: 68−71.

[30] ZHAO M D, FAN X, WANG T J. Fatigue damage of closed-cell aluminium alloy foam: Modelling and mechanisms [J]. International Journal of Fatigue, 2016, 87: 257−265.

[31] KOLLURI M, MUKHERJEE M, GARCIA-MORENO F, BANHART J, RAMAMURTY U. Fatigue of a laterally constrained closed cell aluminum foam [J]. Acta Materialia, 2008, 56: 1114−1125.

[32] LINUL E, SERBAN D A, MARSAVINA L, KOVACIK J. Low-cycle fatigue behavior of ductile closed-cell aluminum alloy foams [J]. Fatigue & Fracture of Engineering Materials & Structures, 2017, 40: 597−604.

[33] LIU P S, DU H Y. Investigation on fatigue property of three-dimensional reticulated porous metal foams [J]. Materials Science and Technology, 2012, 28: 569−575.

[34] INGRAHAM M D, DEMARIA C J, ISSEN K A, MORISSON D J. Low cycle fatigue of aluminum foam [J]. Materials Science and Engineering A, 2009, 504: 50−156.

[35] OLURIN O B, MCCULLOUGH K Y G, FLECK N A, ASHBY M F. Fatigue crack propagation in aluminum alloy foams [J]. International Journal of Fatigue, 2001, 23: 375−382.

[36] FAN X, ZHAO M D, WANG T J. Experimental investigation of the fatigue crack propagation in a closed-cell aluminum alloy foam [J]. Materials Science and Engineering A, 2017, 708: 424−431.

[37] MOTZ C, FRIEDL O, PIPPAN R. Fatigue crack propagation in cellular metals [J]. International Journal of Fatigue, 2005, 27: 1571−1581.

[38] AMSTERDAM E, de HOSSON J T M, ONCK P R. Failure mechanisms of closed-cell aluminium foam under monotonic and cyclic loading [J]. Acta Materialia, 2006, 54: 4465−4472.

[39] VENGATACHALAM B, POH L H, LIU Z S, QIN Q H, SWADDIWUDHIPONG S. Three dimensional modelling of closed-cell aluminium foams with predictive macroscopic behaviour [J]. Mechanics of Materials, 2019,136: 103067.

[40] NAMMI S K, MYLER P, EDWARDS G. Finite element analysis of closed-cell aluminium foam under quasi-static loading [J]. Materials & Design, 2010, 31: 712−722.

[41] CZEKANSKI A, ELBESTAWI M A, MEGUID S A. On the FE modelling of closed-cell aluminium foam [J]. International Journal of Mechanics and Materials in Design, 2005, 2: 23−34.

[42] KADER M A, ISLAM M A, HAZELL P J, ESCOBEDO J P, SAADATFAR M, BROWN A D, APPLEBY-THOMAS G J. Modelling and characterization of cell collapse in aluminium foams during dynamic loading [J]. International Journal of Impact Engineering, 2016, 96: 78−88.

[43] ULBIN M, GLODEŽ S, VESENJAK M, DUARTE I, PODGORNIK B, REN Z, KRAMBERGER J. Low cycle fatigue behaviour of closed-cell aluminium foam [J]. Mechanics of Materials, 2019, 133: 165–173.

[44] ULBIN M, BOROVINŠEK M, HIGA Y, SHIMOJIMA K, VESENJAK M, REN Z. Internal structure characterization of AlSi7 and AlSi10 advanced pore morphology (APM) foam elements [J]. Material Letters, 2014, 136: 416−419.

[45] SIMULIA. FE-safe, user manual [M]. Version 6.5. Dassault Systems, 2014.

[46] DESHPANDE V S, FLECK N A. Isotropic constitutive models for metallic foams [J]. Journal of the Mechanics and Physics of Solids, 2000, 48: 1253−1283.

[47] OKOROKOV V, GORASH Y, MACKENZIE D, RIJSWICK R. New formulation of nonlinear kinematic hardening model. Part II: Cyclic hardening/softening and ratcheting [J]. International Journal of Plasticity, 2019, 122: 244−257.

[48] Abaqus MIT. https://abaqus-docs.mit.edu/2017/English/SIMACAEMATRefMap/simamat-c-hardening.htm#simamat-c-usagecalibration. 2019−11−11.

基于不同材料模型的闭孔泡沫铝疲劳分析

M. ULBIN, S. GLODEŽ

Faculty of Mechanical Engineering, University of Maribor, Smetanova 17, 2000 Maribor, Slovenia

摘　要：使用真实多孔模型和三种均质材料模型(可压缩泡沫模型、等向强化模型和随动强化模型)对 AlSi7 闭孔泡沫铝进行疲劳分析。所用三种均质材料模型的数值分析是基于先前在应力比 R=0.1 的振荡拉伸载荷下进行疲劳测试所得实验结果。计算结果表明，等向强化模型和随动强化模型均适用于分析闭孔泡沫铝的疲劳行为。此外，与等向强化模型相比，随动强化模型所需的模拟时间更短。另一方面，可压缩泡沫模型不适用于拉伸载荷条件下的疲劳分析。

关键词：闭孔泡沫铝；疲劳；数值分析；材料模型

(Edited by Bing YANG)